THE UNIVERSITY of EDINBURGH

Edinburgh Research Explorer

Significance of gas-liquid interfaces for two-phase flows in micro-channels

Citation for published version:
Chao, C, Xu, X, Okachukwu Kwelle, S & Fan, X 2018, 'Significance of gas-liquid interfaces for two-phase flows in micro-channels', *Chemical Engineering Science*, vol. 192, pp. 114-125. https://doi.org/10.1016/j.ces.2018.07.026

Digital Object Identifier (DOI):
10.1016/j.ces.2018.07.026

Link:
Link to publication record in Edinburgh Research Explorer

Document Version:
Peer reviewed version

Published In:
Chemical Engineering Science

General rights
Copyright for the publications made accessible via the Edinburgh Research Explorer is retained by the author(s) and / or other copyright owners and it is a condition of accessing these publications that users recognise and abide by the legal requirements associated with these rights.

Take down policy
The University of Edinburgh has made every reasonable effort to ensure that Edinburgh Research Explorer content complies with UK legislation. If you believe that the public display of this file breaches copyright please contact openaccess@ed.ac.uk providing details, and we will remove access to the work immediately and investigate your claim.

Download date: 05. May. 2023

Significance of two-phase interface in capillary resistance to two-phase flows in micro-channels

Cong Chao, Xu Xu, Stephen Okachukwu Kwelle, Xianfeng Fan*

Institute for Materials and Processes, School of Engineering, The University of Edinburgh, Edinburgh EH9 3JL, UK

Abstract

Investigation was designed to clarify the contribution of two-phase interfaces to capillary resistance, the difference in capillary resistance to single-phase and two-phase flows in micro-channels, and to define the size of an effective pore throat. A new correlation was also derived to predict the resistant pressure to two-phase flows in tapered micro-capillaries. The experimental results indicate that the resistant pressure profile of a capillary for two-phase flows is significantly different from that for single-phase flows. This difference is due to the capillary resistance induced by the gas-water interface. The resistance to the gas-water interface is significantly higher than that to either of the single phases. The 'effective pore throat' of a capillary has been also defined in this study. When a single-phase fluid passes through this 'effective pore throat point' in a tapered capillary, the resistant pressure does not change. However, when a two-phase interface flows through this 'effective pore throat point', the resistant pressure starts to increase sharply. The 'effective pore throat' is different from the geometrical throat of a channel. Comparison of experimental results with various theoretical models has been discussed. The results show that the combination of new-derived correlation and the homogenous flow model or the separated flow model, to some extent, can simulate the pressure drop when the flow path diameter is less than the 'effective pore throat' (within ±20% deviation), but cannot predict the resistant pressure when the diameter of a flow path is greater than the 'effective pore throat'.

Key word: Capillary resistance, Capillary Pressure, Two-phase Flows, Interface, Frictional pressure, Pore throat

1. Introduction

Immiscible two-phase flow in porous media is of great importance to many fields, such as oil recovery [1], CO_2 sequestration [2], water management in fuel cells [3], electronic chips [4], compact heat exchangers [5, 6], biotechnology and microbubbles for drug delivery [7-9]. In many circumstances, the resistant pressure to gas-liquid flows in porous media is used as a criteria to characterize migration and transport processes, and the interaction between microchannel and fluids in a confined space. The resistance to fluids flow in porous media is

* Corresponding author: Tel.: +441316505678; Fax: +441316506551; Email: x.fan@ed.ac.uk

normally controlled by pore structure (such as pore size, pore throat [10-12]), pore surface wettability [13, 14], fluid properties (such as viscosity and surface tension), and the interface of two phases [15]. Numerous investigations have been reported in literature.

However, to the author's best knowledge, there still several important factors have not been clarified in detail. For example, pore throat has been used as a parameter to define the effect of pore structure on two-phase flows, and the resistant pressure. The common method to identify pore throat combines the image-analysis of reservoir planes through X-ray computed microtomography with pore size distribution obtained by mercury injection porosimetry [16-18]. Because a number of throats may be missed when imaging a few sets of parallel planes, the identification of pore throat is still inaccurate [19]. At the pore level, no report has yet clearly defined what pore size can be seen as a throat. Another example is that how two-phase interfaces in porous media affect the resistant pressure to fluids flow. Many Investigations have focused on the effect of channel geometry, size, mass velocities and liquid properties on the frictional pressure drop (one preponderant resistant pressure) for single-phase and two-phase flows in microchannels [20-23]. The simulation of frictional pressure in porous media can also be obtained through Hagen-Poiseuille or Darcy-Weisbach equation [24]. However, no report has demonstrated the contribution of an interface, not a bulk liquid phase, to the resistant pressure.

For fluids flowing in porous media, the resistant pressure is generally formed due to viscous force, capillary force, frictional force and gravitational force. The capillary pressure has been calculated through Young-Laplace equation in dynamic imbibition processes [13, 25, 26]. The frictional pressure to two-phase flows in macroscale channels is commonly estimated by the homogenous flow model and the separated flow model. Those flow models are generally proposed for channels with a diameter greater than 1 mm, and can be applied to predict the frictional pressure drop for two-phase flows in microchannels with the diameter less than 500 μm even though some discrepancies exist [27-29]. In early 1997's, Stanley et al. employed Lockhart and Martinelli correlation to predict the frictional pressure drop for two-phase flows in aluminium tubes with the diameter ranging from 56 to 256 μm [30]. Kawahara et al. reported that Lockhart and Martinelli correlation (taking C value as 0.24) can predict the frictional pressure drop with a deviation of ±10% for nitrogen-water flows in a 100 μm circular horizontal silica tube if gas and liquid superficial velocity are 0.1- 60 m/s and 0.01- 4m/s, respectively [31]. Some new correlations were derived through modifying the parameters used in correlations to meet the individual flow conditions and channel geometry [22, 32, 33].

Many investigations into the resistant pressure to two-phase flows have been conducted at high liquid velocity in channels with the diameter greater than 1 mm [22, 27, 28]. Very little experimental work has been reported to conduct at a low flow velocity. At a high flow velocity, the resistant pressure is mainly caused by viscose force, frictional force, and the contribution of capillary force

to the pressure drop has always been ignored in previous research [34]. However, in most porous media, for example, blood transport in microvessel, gas-fuel and water in fuel cell electrodes, hydrocarbons and CO_2 migration in reservoir rocks, the fluid flow rate is very low, and capillary number, *Ca* in such two-phase flow regimes may be less than 10^{-5}. In these cases, capillary force is a significant contributor to the resistant pressure. For example, blood velocity is ranging from 0.2 mm/s to 2.7 mm/s in arterioles and venules, and the diameter of micro-vessels is in the range of tens to a few hundred microns [35, 36]. Detailed investigation into the resistance of micro-vessels to two-phase flows would help to evaluate the feasibility of microbubbles as a carrier to deliver drugs or gene to a target site, such as, whether microbubbles can overcome the resistance to reach targeted sites; whether microbubbles cause an increase in the local blood pressure. Due to the microscale diameter of capillaries, microbubbles may suffer high resistant pressure. If the resistant pressure is greater than the driving pressure (blood pressure), the resistance may stop microbubbles going further and microbubbles lodge in some place of micro-vessels, causing the vascular blockage. Also, the hydraulic diameter of flow path employed in previous study, no matter for mini- or micro-channels, was always constant. In practice, pore structure is complex and the change in the diameter of flow path is very common in porous media, such as blood vessels (varying from several centimetres to several microns), flow path in soils/aquifers, gas or petroleum reservoirs [24]. How will this change in the diameter of flow path and gradient affect the resistant pressure to fluids flow?

In this study, experiments were designed to investigate the difference in the resistant pressure between single-phase and two-phase flows, the effect of an interface on the resistance, the effect of the diameter along flow path on the resistance, and the effective pore throat. We defined the ‘effective pore throat’ as a diameter at which the resistant pressure starts to increase sharply. The resistant pressure to two-phase flows was also simulated and different models were tested through comparing the predicted results with the experimental data. To fit our experimental capillary geometry, a new correlation was derived based on Darcy-Weisbach equation. Combined with our newly derived equation, the frictional pressure to two-phase flows was predicted through the homogenous flow model and the separated flow model. The capillary pressure was calculated through Young-Laplace equation in which the contact angle was measured directly in glass micro-capillaries based on our previous study [37].

2. Theories and models

Hydraulic resistance to two-phase flows in porous media is determined by the combination of capillary force, buoyancy force, gravity force, viscous or frictional force and interactions among wall materials and fluids. The magnitudes of inertial effects, gravitational forces (or buoyancy force) and viscous force to surface tension are given by the dimensionless numbers as,

$$We = \frac{\rho r u^2}{\gamma} \quad (1)$$

$$Bo = \frac{(\rho_w - \rho_o) g l^2}{\gamma} \quad (2)$$

$$Ca = \frac{\mu u}{\gamma} \quad (3)$$

where *We* is the Weber number, *Bo* is the Bond number and *Ca* is the capillary number. ρ is the fluid density, subscripts *w, o* denoting the wetting and non-wetting phase. *r* is the radius of flow path, u is the fluid superficial velocity, γ is the surface tension. *g* is the gravitational acceleration, l is the characteristic length and μ is the fluid dynamic viscosity.

If *We* and *Bo* are much less than 1 [38], inertial effects and gravitational or buoyancy effects can be neglected [39, 40]. For the case that *Ca* is less than 10^{-5}, the flow is dominated by capillary force. The value of each number in our study is given in Table 1. It indicates that the inertial force can be ignored and the capillary force needs to be considered when fluids flow in a microscopic capillary where *Ca* number is less than 10^{-5}.

Table 1: The value of each parameter in our study

u_l	2.36×10^{-5}- 0.0262 m/s	*Re*	7.96×10^{-5}- 2.65
Ca	2.90×10^{-7}- 3.24×10^{-4}	*We*	4.29×10^{-4}- 4.91×10^{-4}
Bo	1.10×10^{-3}- 1.22	γ (DI water)	72.0 mN/m
γ (air)	1.81×10^{-5} Pa·s)	μ (DI water)	8.94×10^{-4} Pa·s
ρ (air)	1.225 kg/m^3	ρ (DI water)	998.2 kg/m^3

In this experiment, the fluid was pumped into a horizontal tube and flowed with a superficial velocity u_l. The air bubble with a constant volume was injected into the glass tube and moved with a superficial velocity u_g. According to Fairbrother and Stubbs, the velocity of gas phase (bubble) in a tube filled with liquid is a little higher than that of the liquid phase [41]. Bretherton [42] derived an expression, given in equation (4) to calculate the bubble velocity for the flow regime with small Reynolds number, $Ca < 10^{-5}$ and $We \ll 1$.

$$u_g = u_l \left\{ 1 + 1.29 \times \left(3 \frac{\mu u_l}{\gamma} \right)^{\frac{2}{3}} \right\} \quad (4)$$

When a bubble is flowing in a tube filled with liquid, a uniform thin liquid film exists between the tube wall and the gas phase. Due to the negligible of gravitational force and shear force of gas phase, the liquid film is commonly assumed to be stagnant and thus does not contribute to frictional pressure drop [38, 43]. The thickness of the liquid film (*d*) in a circular tube with a dimeter *D*

can be calculated through the correlation proposed by Bretherton [42],

$$\frac{d}{D} = 0.67Ca^{2/3} \quad (5)$$

2.1 Frictional pressure to two-phase flows in a capillary

Two models, the homogeneous flow (HFM) and the separated flow model (SFM), can be used to calculate the frictional pressure to two-phase flows caused by wall friction in a horizontal capillary. The homogeneous flow model averaged fluid properties based on the ratio of liquid and gas components. The separated flow model is based on the individual behavior of each component [44].

In the HFM, the frictional pressure loss for incompressible fluids flowing through a capillary is related to the wall shear stress or the frictional force, which can be calculated through Darcy-Weisbach equation, given by,

$$\Delta P_f = f\frac{\Delta L\rho u^2}{2D} \quad (6)$$

where *L* and *D* are the length and hydraulic diameter of flow path, respectively. u is the mean fluid superficial velocity and f is the Darcy friction factor.

The Darcy-Weisbach equation was derived based on the assumption that the flow regime is one-dimensional flow, i.e., the change of fluid properties across the width of the flow path is negligible compared with the changes along the length of the flow path [44].

For two-phase flows, equation (6) becomes,

$$\Delta P_{TP} = f_{TP}\frac{\Delta L G_m^2}{2\rho_m D} \quad (7)$$

where G_m is the total mass flux and ρ_m is the homogenous mixture density, defined by,

$$\frac{1}{\rho_m} = \frac{x}{\rho_g} + \frac{1-x}{\rho_l} \quad (8)$$

where *x* is the mass quality, defined as $x = \frac{m_g}{m_g+m_l}$, in which *m* is the mass flow rate of gas (*g*) and liquid (*l*). f_{TP} is the two-phase flow frictional factor.

For laminar flow, f_{TP} is obtained from the conventional correlation, gives,

$$f = \frac{64}{Re} \quad (9)$$

and the Reynolds number of mixture is given by,

$$Re_m = \frac{\rho u D}{\mu_m} \quad (10)$$

where μ_m is the mixture viscosity.

In the SFM, Lockhart and Martinelli correlation [45] was commonly used to predict the frictional pressure drop in two-phase flows, $(\Delta P_f)_{TP}$, given as:

$$\left(\frac{\Delta P_f}{\Delta L}\right)_{TP} = \phi^2 (\frac{\Delta P_f}{\Delta L})_{SP} \quad (11)$$

where $(\frac{\Delta P_f}{\Delta L})_{SP}$ is the frictional pressure to single-phase flows in a capillary. ϕ^2 is the two-phase friction multiplier, widely calculated through,

$$\phi^2 = 1 + \frac{C}{X} + \frac{1}{X^2} \quad (12)$$

where Chisholm parameter, *C* is a constant indicating the two-phase flow conditions and ranges from nearly 0 to 21 depending on the channel diameter and mass flowrate. *X* is the Lockhart-Martinelli parameter, given by

$$X^2 = \frac{(\Delta P_f/\Delta L)_l}{(\Delta P_f/\Delta L)_g} \quad (13)$$

$$(\frac{\Delta \mathrm{P}}{\Delta \mathrm{L}})_l = \frac{G^2(1-x)^2 f_l}{2D\rho_l}$$

$$(\frac{\Delta \mathrm{P}}{\Delta \mathrm{L}})_g = \frac{G^2 x^2 f_g}{2D\rho_g}$$

where the subscript *l, g* demoting the gas and liquid.

2.2 Capillary pressure to two-phase flows in a capillary

Along with the frictional pressure discussed above, capillary pressure, P_c needs to be considered for two-phase flows in microscopic capillary. P_c results from the interfacial tension caused by the curvature of interface between two fluids. It is equal to the pressure difference between non-wetting (P_n) and wetting phase (P_w) at equilibrium, given in Young-Laplace equation:

$$P_c = P_n - P_w = \frac{2\gamma}{R} \quad (14)$$

For the case in a cylindrical capillary with a radius r, $r = R \cdot cos\theta$ (θ is the contact angle, R is the spherical meniscus), equation (15) can be derived from Young-Laplace equation:

$$P_c = \frac{2\gamma cos\theta}{r} \quad (15)$$

Equation (15) has been used to describe the capillary pressure at both the equilibrium state and dynamic wetting processes in porous media [13, 25, 26]. However, Equation (15) was proposed mainly for the equilibrium state. To achieve more acceptable results for the capillary pressure calculated from Equation (15), in this study, the contact angle is substituted by the dynamic contact angle measured previously in glass capillaries with the diameter ranging from 100-1000 μm [46].

2.3 Pressure loss of sudden contraction

The sudden contraction in tube diameter would cause a small pressure drop when fluids flow in tubes. In this study, we assume a sudden geometry contraction occurs at a point with a diameter D_t. For two-phase flows, the pressure drop due to the sudden contraction, $\Delta P_{contraction}$ is given by [47],

$$\Delta P_{contraction} = \frac{G^2}{2\rho_l}\left[\left(\frac{1}{C_C}-1\right)^2 + 1 - K^2\right]\left[1 + x\left(\frac{\rho_l}{\rho_g}-1\right)\right] \quad (16)$$

where *G* is the total mass flux of fluids. *K* is the ratio between the cross-sectional area of the contraction point (with a diameter D_t) to the area of the glass tube with an inner diameter of 3 mm. C_c is the contraction coefficient, which can be estimated from the function of *K*, given by [48],

$$C_C = \frac{1}{0.639(1-K)^{0.5}+1} \quad (17)$$

2.4 Overall resistant pressure to two-phase flows in a capillary

The overall resistant pressure to fluids flow in a microscopic capillary should contain the frictional pressure, capillary pressure and contraction pressure loss. In a single or two-phase flow regime, no heat transfer is involved, therefore, the acceleration pressure drop of fluid flow can be ignored [32]. Also, not like those investigations focusing on the liquid penetration into porous media where the capillary force is the driving force to push fluid to move into a capillary [25, 49, 50], the capillary force in present experiment is a resistance to fluid flow.

The overall resistant pressure to fluid flow in the glass tube with an inner diameter of 3 mm and a tapered capillary as shown in Fig. 1 is given by,

$$\Delta P = \Delta P_{f1} + \Delta P_{f2} + \Delta P_c + \Delta P_{contration} - \frac{\rho}{2}(u_1^2 - u_2^2) \quad (18)$$

where ΔP_{f1} is the frictional pressure drop in the tube with an inner diamter of 3 mm, ΔP_{f2} is the frictional pressure drop for fluid flowing through the tapered capillary, $\Delta P_{contration}$ is the pressure loss due to the sudden contraction and ΔP_c is the capillary pressure. u_1 and u_2 are the mean fluid superficial velocity in the tube with an inner diameter of 3 mm and at the tip point of a tapered capillary, respectively.

For ΔP_{f1}, the resistant pressure to a gas-liquid interface (an elongated bubble) in the tube with a constant diameter, contains three components: (1) the frictional pressure drop for liquid flow, ΔP_{fl}; (2) the pressure drop over a single gas bubble due to the existence of the interfacial tension across the caps of bubble, ΔP_b; (3) the frictional pressure drop in the gas phase, ΔP_g, i.e.,

$$\Delta P_{f1} = \Delta P_b + \Delta P_{fl} + \Delta P_g \quad (19)$$

Due to the large difference between the viscosity of gas and liquid, we ignore the frictional pressure drop in the gas phase. The frictional pressure drop for

liquid, ΔP_l can be calculated through equation (7). The pressure drop over a single gas bubble, ΔP_b was given by Bretherton [42],

$$\Delta P_b = 7.16(3Ca)^{2/3}\frac{\gamma}{D} \quad (20)$$

After an interface enters the tapered capillary, it moves with inconstant velocity as the capillary diameter decreases at a constant gradient. A new correlation was derived based on Darcy-Weisbach equation to fit our geometry, which was discussed in 4.3.1. Both the homogenous flow model and the separated flow model were combined with new-derived correlation to calculate the frictional pressure drop for two-phase flows. The resistant pressure was predicted through combining equation (18) with equations (15) and (16), and the predicted results were compared with the experimental data to test the accuracy of new-derived correlation and different flow models.

3. Methods and materials

3.1 Manufacturing the tapered capillaries

Tapered capillaries with various size and gradients were made from standard cylindrical glass tubes (borosilicate, bore size 3 mm, 0.5 m long, 6 mm (ext.) diameter; FB51467 Fisher Scientific, UK). The glass tubes were firstly cut into 12 cm tubes. The borosilicate glass is highly hydrophilic, and high cleaned conditions were required in the whole manufacture and measurement processes. The glass tubes were washed using 5M sodium hydroxide solution (Fisher Scientific) and acetone (Fisher Scientific, A/0600/15), and rinsed thoroughly with deionized water (C540 Deionizer, Veolia Water Solutions Technologies). The cleaned glass tubes were then heated up to 550 °C on butane flame (butane Battery, D2-BS 0617) to remove any organic residue and kept in the dust-proof enclosure. Tapered capillaries with various size were obtained through melting the middle section of the clean glass tubes on flame and pulling the middle section into capillaries with suitable size. The length of all tapered capillaries was fixed at about 3.5 cm. The inner diameter of tapered capillary was measured under a microscope. The tapered capillary was marked to identify the position of the gas-liquid interface corresponding to the measured resistant pressure.

3.2 Measurement of resistant pressure to fluid flow in tapered capillaries

The experiment setup, as shown in Fig.1, contains a liquid delivery pump (LC-20 AD, Shimadzu), a digital pressure transducer (DPI 280, Druck) with the resolution of 0.01 mbar to measure resistant pressure, a long working distance microscope (Brunel Microscope Ltd, 10x objective) fitted with a digital camera (AM7023 Dino-Eye, Dino-Lite Digital Microscope) to record the interface motion in tapered capillaries. The elapsed time and the resistant pressure were recorded with a time interval of approximate 0.25 s and displayed on the

computer through a LabView software.

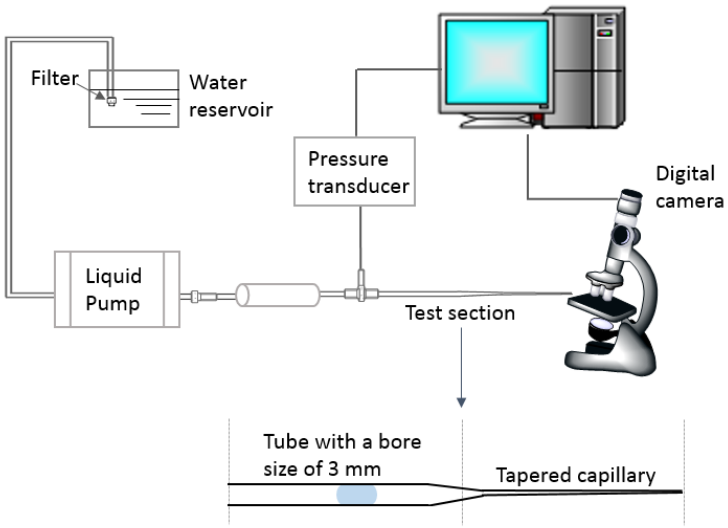

Fig. 1 Experimental apparatus

To measure the resistant pressure to two-phase flows, a tapered capillary was initially filled with deionized water and then air with a fixed volume was injected through a clean and sterile syringe to create a gas-liquid interface. The length of tapered capillary is generally controlled at 3.5 cm and the volume of air was controlled at 0.05± 0.005 ml. The deionized water was pumped from a water reservoir through a filter to ensure that no solid contaminants would block the fluid flow line. The movement of an interface and the diameter of the marked point at which an interface flows through were imaged by the microscope and digital camera. Since the accuracy of measured flow path diameter depends on the measurement method and image quality, a LED light was located under the capillary to light the inner boundary line of glass capillary and to reduce the image distortion [51]. The entire experimental process was conducted on a vibration-free horizontal workstation to minimize the external effects on measurement. All experiments were performed at room temperature and atmospheric pressure. Sufficient time was allowed to collect data to ensure equilibrium state would be achieved and the measurement of the resistant pressure were repeated three times for all capillaries.

4. Results and discussions

4.1 Difference in resistant pressure profiles for single-phase and two-phase flows

To compare the resistant pressure profiles for a single-phase flow and a two-phase flow in the tapered capillary, water flow rate was controlled at constant. The typical resistant pressure profiles for water flows and for gas-water flows in tapered capillaries are presented in Figs. 2, 3 and 4. The results indicate that the resistant pressure profile for a two-phase flow is significantly different from that for a single-phase flow. For a single-phase flow, the resistant pressure took

a constant value once the flow reached an equilibrium (Figs. 2a and 3a). For a two-phase flow, the pressure profile can be divided into two sections which are separated by a critical pore diameter as shown in Figs. 2b, 3b and Fig. 4. The resistant pressure varied with the position of the gas-water interface in the capillary. Before the gas-water interface entered the capillary with a diameter less than the critical size, the resistant pressure profile for a two-phase flow did not change with pore size and was almost the same as the pressure profile for a single-phase flow. Once the gas-water interface reached the capillary with a diameter less than the critical size, a sharp increase at a constant rate in the resistant pressure was observed. This 'sharp increase' was due to the capillary resistance to the gas-water interface, rather than to the phase body. The resistance to the gas-water interface was much higher than that to the single-phase or the phase body. This is a phenomenon that we observed and has not been reported in literature.

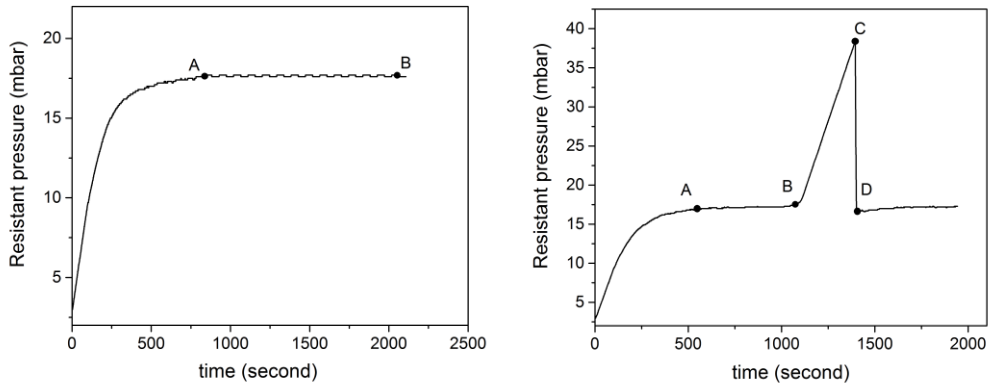

Fig. 2. Resistant pressure profiles for (a) the single-phase (water) flow and (b) the two-phase flow in a tapered capillary with a tip size of 131 μm

Fig. 2a shows the resistant pressure profile for a single-phase flow in a capillary with a tip size of 113 μm. The pressure increased linearly at the beginning (from 0 s to nearly 1000 s), and then slowly reached the equilibrium and kept the balance after the point A. The fluid inside the capillary was driven by the pumped deionised water with a constant flowrate to overcome the resistant force, which was mainly caused by the capillary force and viscous force. During the acceleration section, the viscous force increased as it is proportional to the velocity. When fluid velocity in the capillary was near to that of the pumped deionised water, and the force balance was established, the resistant pressure (see the section AB) to water flow was balanced and took a constant value.

The resistant pressure profile for two-phase flows in a tapered capillary with a tip size of 130 μm is shown in Fig. 2b. The gas-water interface was driven by the water flow, and finally came out from the capillary tip. Before the gas-water interface reached the critical point B in Fig. 2b, the resistant pressure profile of two-phase flows was the same as that for single-phase flows. The resistant

pressure increased at the initial stage, and then remained balanced after the point A. After the point B, the resistant pressure started to increase dramatically at a constant rate until the interface flowed out from the capillary tip (the point C). In section 4.2, we name this point B as the ‘effective pore throat’, at which the resistant pressure to the gas-water interface took effect and the measured resistant pressure suddenly increased. Once the interface came out from the capillary, the pressure deeply dropped to the point D. After that, only water flowed inside the capillary, and the pressure curve went to balance quickly.

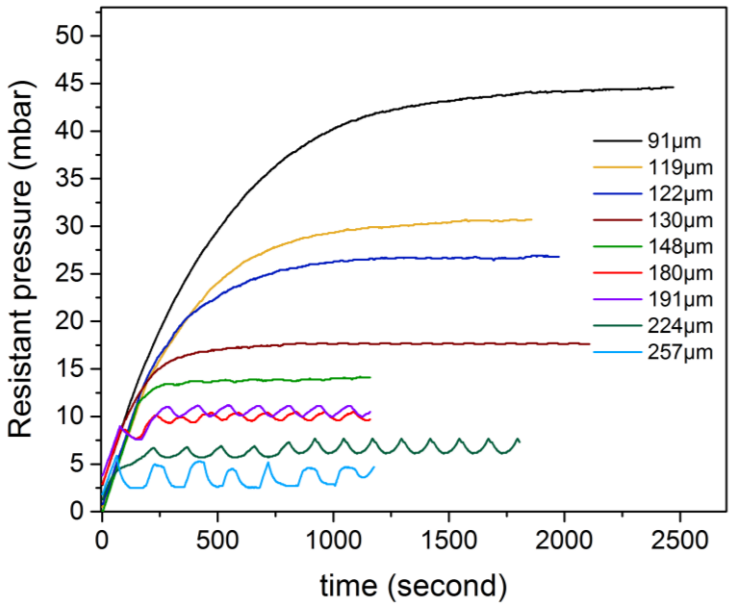

(a)

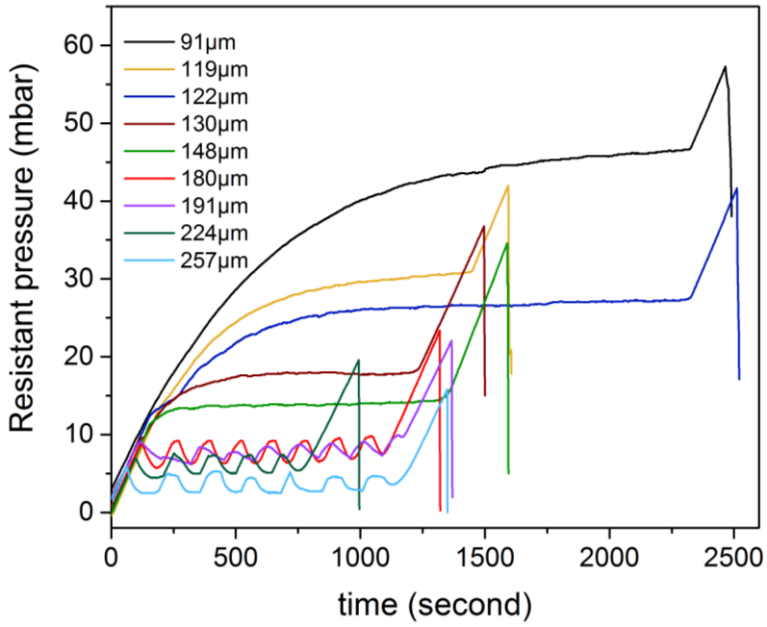

(b)

Fig. 3. Resistant pressure profiles for (a) single-phase (water) flows and (b) two-phase flows in tapered capillaries with tip size ranging from 91-257 μm

Tapered capillaries with tip size from 91 to 257 μm were used to investigate the effect of capillary size on the resistant pressure profiles for single- and two-phase flows at the driving flowrate of 0.01 ml/min. Fig. 3a indicates that at the equilibrium state, the resistant pressure to water phase decreased significantly with the increase in the capillary tip size under the same fluid flowrate. This was due to that both viscous force and capillary force are proportional to the 1/r. Within the large flow path, the resistant pressure drop induced by viscous effect and capillary effect was thus getting smaller.

For two-phase flows, as shown in Fig. 3b, all resistant pressure profiles have the sharp increase once the gas-water interface reached the effective pore throat point. However, single-phase flows did not show this pressure increase phenomenon. The main reason was that the air-water interface would induce capillary force, and this capillary force dominated the flow motion once the capillary diameter was smaller than the effective pore throat and water flow rate is low. According to Young-Laplace equation, the capillary pressure becomes significant when the radius of the capillary is at the microscale. For the air-water flow with the volumetric flow rate of 0.01 ml/min, the capillary pressure was 1.81 mbar (dynamic contact angle, θ=20º) when the interface moved along a capillary with a radius of 1490 μm, while the capillary pressure would be 19 mbar if the capillary radius reduced to 130 μm.

The difference in the pressure drop between single-phase flow and two-phase flow may be explained based on water saturation. For single-phase flows, the wetting fluid (water) was at its maximum saturation (the water was fully filled in a capillary tube), and the saturation of the non-wetting fluid (air) was nearly zero, i.e. S_{nw}=0. Because the dynamic capillary pressure in porous media is the increasing function of the non-wetting phase saturation, the capillary pressure of single-phase flow equals to zero, i.e. $P_c=P_c(S_{nw})=0$ [26]. Therefore, there was no increase in resistant pressure observed when single-phase flows in the capillary even after the effective pore throat. However, both these theories cannot explain this sudden increase in the resistant pressure when interface reaches the effective pore throat.

Some noises at a magnitude of 0.4- 0.5 mbar around the central line were observed in the pressure profiles when capillaries with large tip size (i.e. 180, 191, 224, 257 μm) were used. This fluctuation was caused by the low fluid flow rate, the resolution of pressure transducer, the geometry of the tapered capillary and the fluid surface tension. When fluid reached the capillary tip, a droplet adhered to the capillary tip until the gravity of droplet was greater than the adhesion force between water molecule and glass capillary wall. The fluid droplet at the tip of the capillary generated a small capillary pressure. From the moment a droplet was formed, the resistant pressure started to slightly increase. Once a droplet dripped from the capillary tip, the resistant pressure would decrease and the noise of a pressure profile was thus observed. For capillaries with large tip size, the resistant pressure was so small that the small fluctuation became obvious for the pressure profile. In capillaries with a small tip size,

noises in profiles were not clear as the overall resistant pressure was high.

4.2 Effective pore throat

To investigate the point at which the resistant pressure to an interface takes effect, the resistant pressure versus the capillary diameter was plotted in Fig. 4. The diameter of the capillary body was obtained through processing micrographs corresponding to the measured pressure on each marked point on the tapered capillaries. Due to the geometry of the tapered capillary, the diameter of flow path continuously decreases towards the tip of the capillaries. It clearly shows from Fig. 4 that the capillary diameter significantly affected the resistant pressure to an interface, but not to a single phase. Before an interface met the point P, the resistant pressure to two-phase flows was the same as the pressure for single-phase flows. When the interface reached the point P, the resistant pressure started to increase sharply. We define this point as the 'effective pore throat'.

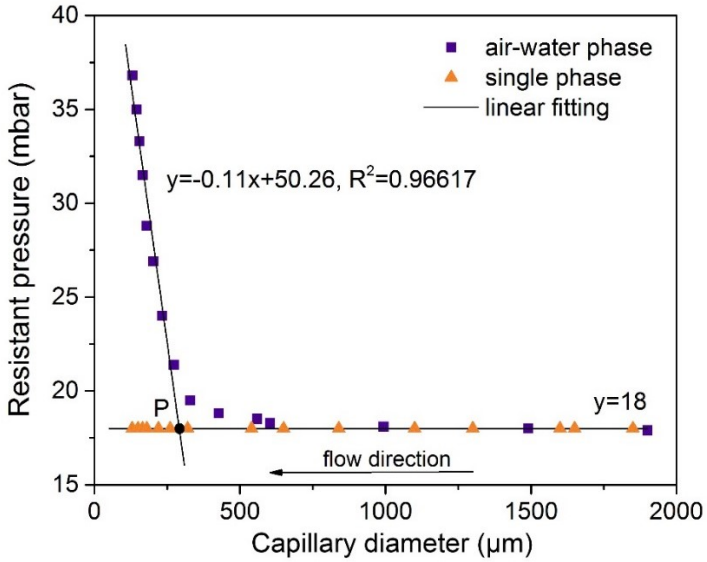

Fig. 4. Resistant pressure versus the capillary diameter for the air-water phase flow and the single-phase flow in a tapered capillary with a tip size of 130 μm

To identify the effective pore throat, the point P in Fig. 4, two simultaneous equations were obtained through linear fitting using Origin software,

$y=-0.11x+50.26$

$y=18$

The intersection of the two lines is the effective pore throat, which is 293 μm for this 130 μm tapered capillary. When the two-phase fluid moved along the flow path with a diameter greater than the effective pore throat, for example, greater than 293 μm for this tapered capillary with a tip size of 130 μm, the resistant pressure to the gas-water interface would be almost zero. This can be clearly seen through comparing the resistant pressure to the single-phase flow and the two-phase flow in the same large section in Figs. 4 and 5. If the size of flow path is smaller than 293 μm, the capillary would offer a significant resistance to

the two-phase interface.

Fig. 5 shows that this particular point exists in all capillaries with tip size ranging from 91 μm to 257 μm, but only for two-phase flows, not for single-phase flows. Similar to Fig. 4, the resistance to two-phase flows started to increase after an interface met the effective pore throat. This cannot be modelled by existing correlations as discussed in the Section 4.3.3. In this study, the resistant pressure mainly is the sum of capillary pressure and frictional pressure. We assume that the frictional pressure to gas phase is negligible. From the resistance to the single phase, it can be seen that the frictional pressure to water phase is constant when water flows through a tapered capillary. Once the interface is introduced, a sharp increase in the resistant pressure at the critical point can be observed from all of the experiments. Theoretically, this sharp increase after the critical point should be due to capillary resistance, as $P \propto \frac{1}{r}$. However, the capillary pressure to the interface is zero when the capillary diameter is slightly larger than the critical point. Therefore, we define this critical point as an effective pore throat. When the capillary diameter is less than the effective pore throat, the capillary force to the interface takes effect.

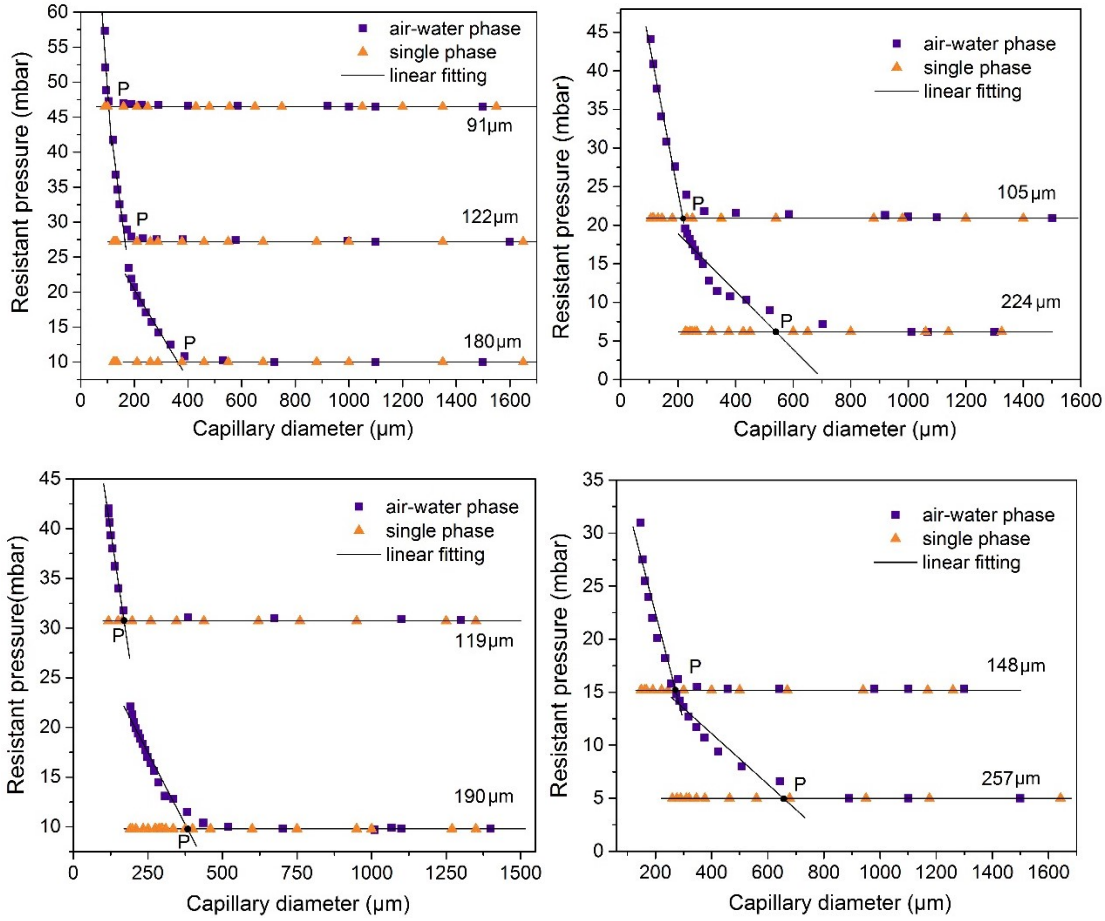

Fig. 5. Resistant pressure versus capillary diameter to single-phase and air-water phase flows in nine tapered capillaries with tip size ranging from 91 μm to 257 μm

It is interesting to notice that the smaller the tip size of a tapered capillary, such as 91 μm, 105 μm, 119 μm and 122 μm, the shaper the increase rate of resistant pressure would be. For tapered capillaries with larger tip size, such as 180 μm, 191 μm, 224 μm and 257 μm, the resistant pressure increased at a relatively gentle rate after an interface passed through the effective pore throat. The size of the effective pore throat varies with the tip size of tapered capillaries. The effective pore throat size versus the tip diameter of capillaries was plotted in Fig. 6. It clearly shows that the larger the tip size is, the larger the effective pore throat size would be. This is in good agreement with the result obtained by Zou et al. [17]. They measured pore throat diameter of sandstone core samples and found that the pore throat size increased with the pore diameter of sandstone. Needs to mention that, this effective pore throat only exists in microscopic capillaries. The flow path with a diameter greater than 870 μm barely has this 'sharp increase in resistant pressure' and the effective pore throat.

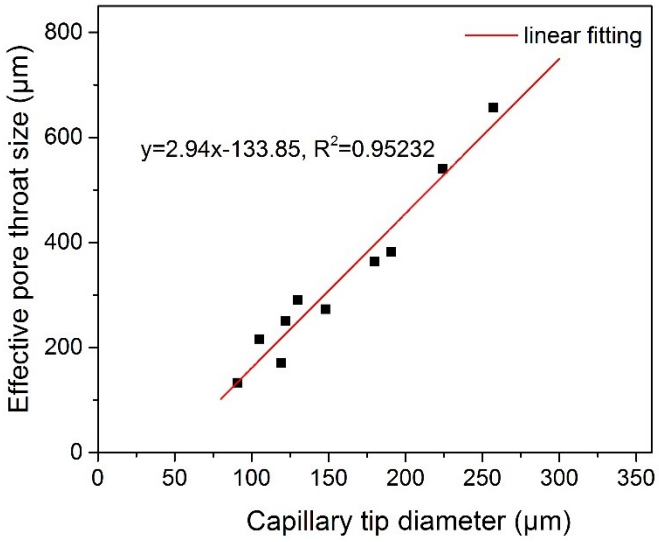

Fig. 6. Effective pore throat versus capillary tip diameter

4.3 Simulation of resistant pressure to two-phase flows in tapered capillaries

4.3.1 Derived frictional pressure equation based on Darcy-Weisbach equation

The Darcy-Weisbach equation is used to calculate the frictional pressure drop to fluids flow in channels with a constant diameter. In our experiments, the diameter of tapered capillaries is not constant and the geometry of tapered capillary is actually a circular truncated cone. In order to fit the tapered capillaries use in our experiments, we derived a new correlation based on Darcy-Weisbach equation to calculate the frictional pressure loss.

$$u = \frac{Q}{A} = \frac{Q}{\pi r^2} \tag{21}$$

We assume that the capillary diameter is decreased at a constant gradient, *k*, defined as:

$$k = (r_{et} - r_{tip})/L \tag{22}$$

where r_{et} and r_{tip} are the radius of the effective pore throat and the capillary tip, respectively. *L* is the capillary length from the effective pore throat point to the tip.

$$l = (r_{et} - r)/k \tag{23}$$

where l is the distance of an interface to the point with the radius *r*, differentiating equation (23), gives,

$$dl = -\frac{1}{k}dr \tag{24}$$

Substituting equations (21) and (24) into equation (6), gives

$$\sum P_f = \int -\frac{f\rho Q^2}{4k\pi^2 r^5}dr \tag{25}$$

Integrating equation (25), gives,

$$\Delta P_f = \frac{f\rho Q^2}{\pi^2 k r^4} \tag{26}$$

This new derived equation (26) can be used to calculate the frictional pressure drop for fluid flow in tapered capillaries.

4.3.2 Simulation of frictional pressure to two-phase flows in tapered capillaries

In the HFM, combining the new derived equation (26) with equations (9) and (10), the frictional pressure drop for two-phase flows is given as:

$$\Delta P_{TP} = \frac{f_{TP}\rho_m Q^2}{\pi^2 k r^4} = 32\frac{\mu_m Q}{\pi k r^3} \tag{27}$$

To evaluate the two-phase mixture viscosity, μ_m, numerous models (given in Table 2) have been proposed to fit the particular flow conditions in terms of the hydraulic diameter of the channel and fluids types [52]. The frictional pressure drop to two-phase flows can be obtained through substituting mixture viscosity calculated by different models into equation (27).

Table 2: Dynamic viscosity models for two-phase flows

Authors	Correlations
McAdams [53]	$\frac{1}{\mu_m}=\frac{x}{\mu_g}+\frac{1-x}{\mu_l}$
Cicchitti et al. [54]	$\mu_m=x\mu_g+(1-x)\mu_l$
Dukler et al. [55]	$\mu_m=\beta\mu_g+(1-\beta)\mu_l;\ \ \beta=\frac{Q_g}{Q_g+Q_l}$, *Q* is the volumetric flow rate of gas (*g*) and liquid (*l*).
Beattie and Whalley [56]	$\mu_m=\beta\mu_g+(1-\beta)(1+2.5\beta)\mu_l$
Lin et al. [57]	$\mu_m=\frac{\mu_l\mu_g}{\mu_g+x^{1.4}(\mu_l-\mu_g)}$

In the SFM, the frictional pressure drop for two-phase flows in tapered capillaries can be obtained through combining our new derived equation (26) with equation (11), i.e.,

$$\Delta P_{TP}=\phi^2\Delta P_{SP}=\phi^2\frac{f\rho_l Q^2}{\pi^2 kr^4} \tag{28}$$

where ϕ^2 is determined by the constant *C* according to equation (12), and C is the main parameter to influence the accuracy of the SFM. Most previous studies have been conducted under the condition where the Re number was less than 1000 and the *C* value was 5. However, according to Chung and Kawaji [27], Yue, et al. [28], Saisorn and Wongwises [22], *C* value of 5 gave a large deviation to the predicted pressure for two-phase flows in microchannels. To reduce this deviation, Mishima and Hibiki [58], English and Kandlikar [33] treated *C* value as the function of channel hydraulic diameter. Lee and Lee [32] took into account the effect of mass velocity, hydraulic diameter and surface tension on the two-phase flows in microchannels, and proposed equation (29) to calculate parameter *C*.

$$C=A\lambda^q\psi^r Re_l^s \tag{29}$$

where λ and ψ were defined by Suo and Griffith [59] as,

$$\lambda=\frac{\mu_l^2}{\rho_l\sigma D} \tag{30}$$

$$\psi=\frac{\mu_l u_l}{\sigma} \tag{31}$$

In equation (29), *A*, *q*, *r*, *s* are constants. Saisorn and Wongwises [22] obtained the value of four parameters based on the experimental data conducted in cylindrical capillaries made of fused silica with an inner diameter of 150 μm, gives,

$$C=7.599*10^{-3}\lambda^{-0.631}\psi^{0.005}Re_l^{-0.008} \tag{32}$$

In our simulations, the frictional pressure drop for two-phase flows in tapered capillaries was predicted through combining the new derived equation (26) with:

(1) the homogeneous flow model with different viscosity models; (2) the separated flow model with the *C* value calculated through equation (32).

4.3.3 Simulation of resistant pressure to two-phase flows in tapered capillaries

To predict the overall resistant pressure to two-phase flows in microscopic capillaries, only frictional pressure and capillary pressure drop were considered in this study, as $\Delta P_{contraction}$, ΔP_{f1} and $\frac{\rho}{2}(u_1^2 - u_2^2)$ in equation (18) were calculated based on equations (16) (19) and (20) to be very small. For example, for a capillary with a tip size of 130 μm and the effective pore throat size of 293 μm, $\Delta P_{contraction}$, ΔP_{f1} and $\frac{\rho}{2}(u_1^2 - u_2^2)$ were only 7.7×10^{-6}, 4.0×10^{-4} and 7.9×10^{-4} mbar, respectively. They were extremely small in comparison with the capillary pressure and frictional pressure drop, therefore could be neglected. According to equations (4) and (5), since the *Ca* is less than 3.24×10^{-4} in this study (as shown in Table 1), the superficial velocity of an interface can be assumed to be the same as the liquid velocity and the thickness of the liquid film near the capillary wall, *d*, is negligible, which means the effective flow path diameter is equal to the capillary diameter.

The predicted overall resistant pressure was obtained by adding up the capillary pressure drop and frictional pressure drop. Fig. 7 shows the comparison of the measured resistant pressure with the predicted pressure for two-phase flows in a capillary with a tip size of 130 μm. From Fig. 7, it can be seen that the simulated pressure profiles give a smooth curve, and decrease with the increase of capillary diameter. While, the measured pressure profiles (the hollow hexagon) present the effective pore throat, which separates the profiles into two sections. The resistant pressure does not change before the effective pore throat, but increases sharply after the effective point. As shown in the simulated curves in Fig. 7, no matter the Young-Laplace equation or Darcy-Weisbach equation, the pressure drop calculated from them is reciprocal to the diameter of flow path, even though for flow path with a diameter greater than the effective throat.

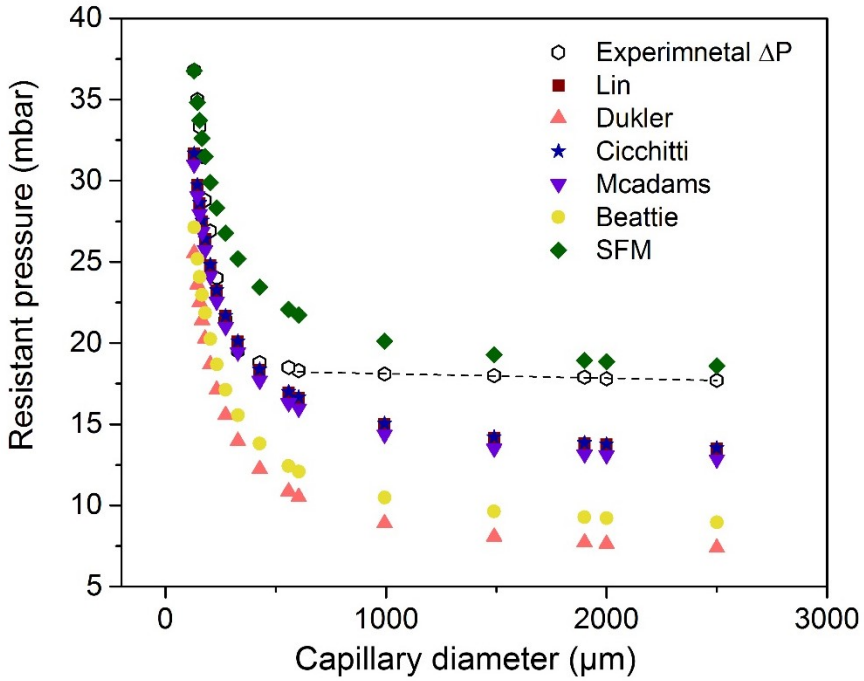

Fig.7. Predicted and experimental resistant pressure with the flow path diameter in a tapered capillary with a tip size of 130 μm

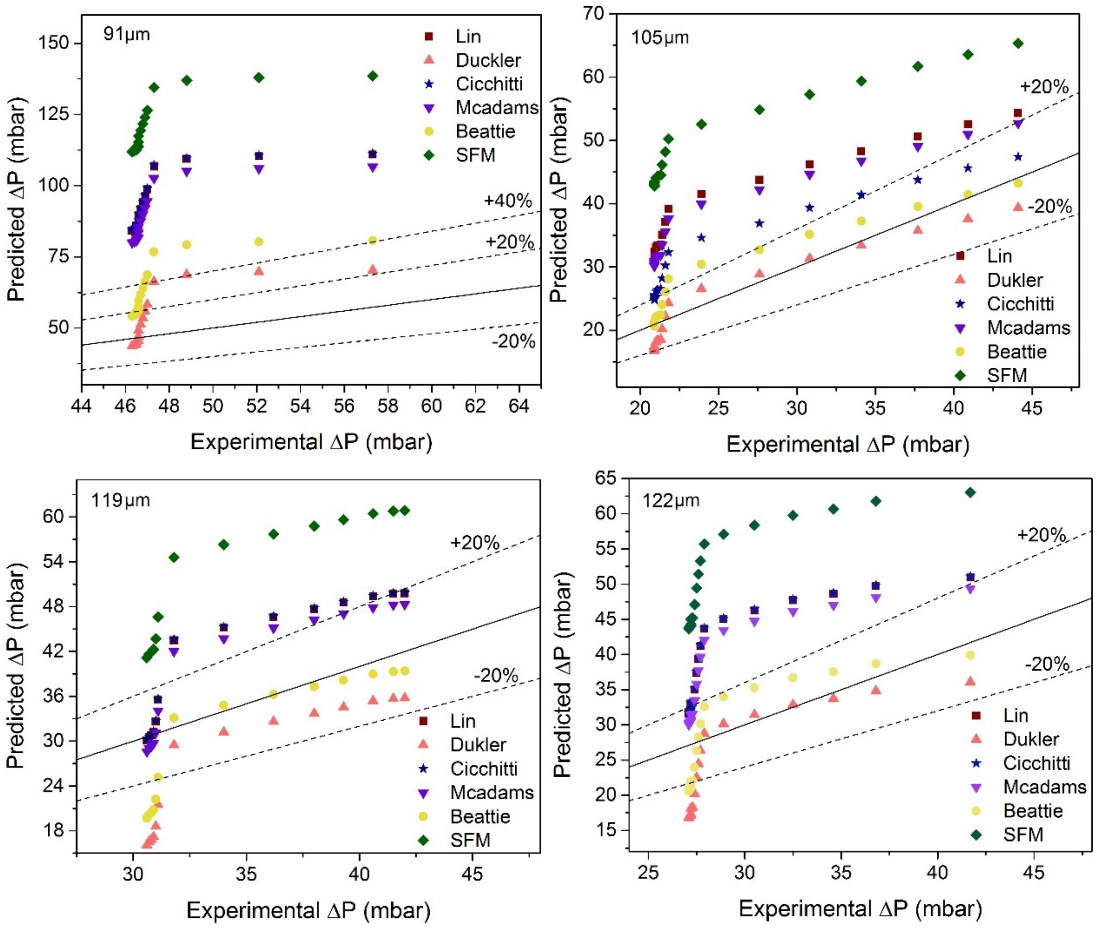

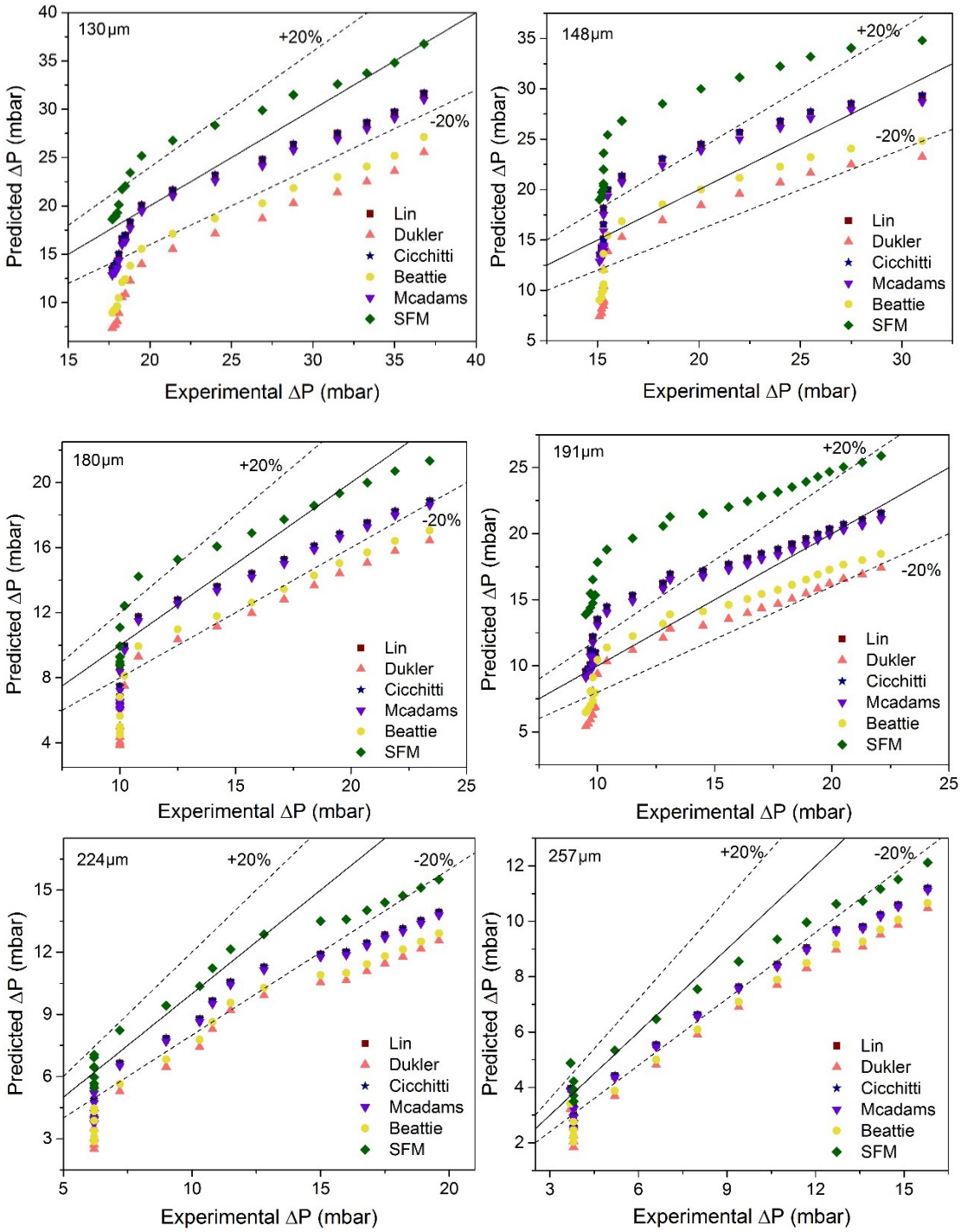

Fig. 8. Experimental pressure drop versus the predicted pressure for two-phase flows in tapered capillaries with tip size ranging from 91 to 257 μm

To evaluate the predictions of resistant pressure in tapered micro-capillaries, the predicted pressure was plotted against the experimental results for all capillaries in Fig. 8. The results indicate that the homogenous flow model (HFM) combined with Beattie model and Dukler model can be used for capillaries with a tip diameter ranging from 91 to 122 μm, and the deviation of prediction is ±20%. Similar results predicted through Dukler viscosity model were also

reported by Kawahara et al. for gas-water flows in a 100 μm circular fused silica tube [31]. Other three models proposed by Lin et al., Cicchitti et al. and Mcadams et al. over-predicted the pressure drop for two-phase flows in tapered capillaries with the tip size smaller than 122 μm.

The separated flow model (SFM) with the *C* value calculated through Lee's correlation (equation (29)) highly over-predicted the resistant pressure drop for the capillaries with tip diameter ranging from 91 to 191 μm. For capillaries with a large diameter, such as 224 and 257 μm, the SFM gave a good prediction with a deviation of ±20%. The accuracy of SFM prediction is directly influenced by the parameter *C*, which is dependent on fluid velocity and capillary diameter [27, 60]. The *C* value used in this study was evaluated based on Saisorn and Wongwises experiments which were conducted at a high superficial liquid velocity (0.37-42.36 m/s) in capillaries with diameters of 150, 220 and 530 μm. While the maximum velocity in our study was about 0.0262 m/s, the actual *C* value should be smaller than the value evaluated through Saisorn and Wongwises experiments. Therefore, an applicable *C* value for the present experimental conditions may make SFM more suitable for two-phase flows in micro-capillaries.

5. Conclusions

In this study, experimental measurements have been designed to investigate the difference in the resistant pressure to single-phase flows and to two-phase flows in micro-capillaries with tip size ranging from 91 to 257 μm and under a constant volumetric flow rate of 0.01 ml/min. The simulation was also conducted to predict the resistant pressure for two-phase flows in capillaries.

The results indicate that the resistant pressure to two-phase flows in tapered capillaries is significantly different from that to single-phase flows. The difference is mainly due to the resistance to the gas-water interface, rather than the phase body. For a single-phase flow, the resistant pressure takes a constant value once the flow acceleration is zero. For a two-phase flow, the resistant pressure profile is equal to the resistance to the single-phase flow, plus the resistance to the gas-water interface. There is a particular point on the capillary. Before the gas-water interface reaches this particular point, the resistance to the gas-water interface is zero. After this point, the resistance to the interface increase sharply. We define this point as the 'effective pore throat'. There is no effective pore throat for a single-phase flow.

Simulation can generally predict the overall resistant pressure for two-phase flows, but cannot match the whole pressure profiles. Current theory cannot explain why the effective pore throat occurs. The homogeneous flow model coupled with Dukler viscosity correlation is able to predict the resistant pressure within a deviation of ±20% for two-phase flows in tapered capillary with tip size from 91 to 122 μm under a low volumetric flow rate. The separated flow model would be more suitable to predict the resistant pressure drop for capillaries with

larger tip size, i.e. 224 and 257 μm.

References

[1] P.S. Ringrose, K.S. Sorbie, P.W.M. Corbett, J.L. Jensen, Immiscible flow behaviour in laminated and cross-bedded sandstones, J. Pet. Sci. Eng. 9 (1993) 103-124.

[2] V. Cvetkovic, G. Dagan, Reactive Transport and Immiscible Flow in Geological Media. II. Applications, Proc. R. Soc. A-Math. Phys. Eng. Sci. 452 (1996) 303-328.

[3] P. Quan, M.C. Lai, Numerical study of water management in the air flow channel of a PEM fuel cell cathode, J. Power Sources 164 (2007) 222-237.

[4] Z. Lian, K. Jae-Mo, J. Linan, M. Asheghi, K.E. Goodson, J.G. Santiago, T.W. Kenny, Measurements and modeling of two-phase flow in microchannels with nearly constant heat flux boundary conditions, J. Microelectromech. Syst. 11 (2002) 12-19.

[5] A. Marchitto, F. Devia, M. Fossa, G. Guglielmini, C. Schenone, Experiments on two-phase flow distribution inside parallel channels of compact heat exchangers, Int. J. Multiph. Flow 34 (2008) 128-144.

[6] S. Vist, J. Pettersen, Two-phase flow distribution in compact heat exchanger manifolds, Exp. Therm. Fluid Sci. 28 (2004) 209-215.

[7] C. Oddou, T. Lemaire, J. Pierre, B. David, Hydrodynamics in Porous Media with Applications to Tissue Engineering, in: K.Vafai (Ed.) Porous Media: Applications in Biological Systems and Biotechnology, CRC Press, 2011, pp. 75-119.

[8] R. Wu, A. Kharaghani, E. Tsotsas, Two-phase flow with capillary valve effect in porous media, Chem. Eng. Sci. 139 (2016) 241-248.

[9] R. Parmar, S.K. Majumder, Microbubble generation and microbubble-aided transport process intensification-A state-of-the-art report, Chem. Eng. Process. 64 (2013) 79-97.

[10] J.S. Wu, B.M. Yu, A fractal resistance model for flow through porous media, Int. J. Heat Mass Transf. 50 (2007) 3925-3932.

[11] J. Yu, X.J. Hu, Y. Huang, A modification of the bubble-point method to determine the pore-mouth size distribution of porous materials, Sep. Purif. Technol. 70 (2010) 314-319.

[12] W.R. Rossen, P.A. Gauglitz, Percolation Theory of Creation and Mobilization of Foams in Porous-Media, AICHE J. 36 (1990) 1176-1188.

[13] P.C. Reeves, M.A. Celia, A functional relationship between capillary pressure, saturation, and interfacial area as revealed by a pore-scale network model, Water Resour. Res. 32 (1996) 2345-2358.

[14] C. Choi, D.I. Yu, M. Kim, Surface wettability effect on flow pattern and pressure drop in adiabatic two-phase flows in rectangular microchannels with T-junction mixer, Exp. Therm. Fluid Sci. 35 (2011) 1086-1096.

[15] C.Y. Lee, S.Y. Lee, Pressure drop of two-phase plug flow in round mini-

channels: Influence of surface wettability, Exp. Therm. Fluid Sci. 32 (2008) 1716-1722.
[16] P.H. Nelson, Pore-throat sizes in sandstones, tight sandstones, and shales, AAPG Bull. 93 (2009) 329-340.
[17] C.N. Zou, R.K. Zhu, K.Y. Liu, L. Su, B. Bai, X.X. Zhang, X.J. Yuan, J. Wang, Tight gas sandstone reservoirs in China: characteristics and recognition criteria, J. Pet. Sci. Eng. 88-89 (2012) 82-91.
[18] W.B. Lindquist, A. Venkatarangan, J. Dunsmuir, T.F. Wong, Pore and throat size distributions measured from synchrotron X-ray tomographic images of Fontainebleau sandstones, J. Geophys. Res-Solid Earth 105 (2000) 21509-21527.
[19] S. Peng, Q.H. Hu, S. Dultz, M. Zhang, Using X-ray computed tomography in pore structure characterization for a Berea sandstone: Resolution effect, J. Hydrol. 472 (2012) 254-261.
[20] G. Ribatski, A Critical Overview on the Recent Literature Concerning Flow Boiling and Two-Phase Flows Inside Micro-Scale Channels, Exp. Heat Transf. 26 (2013) 198-246.
[21] A. López-Belchí, F. Illán-Gómez, F. Vera-García, J.R. García-Cascales, Experimental condensing two-phase frictional pressure drop inside mini-channels. Comparisons and new model development, Int. J. Heat Mass Transf. 75 (2014) 581-591.
[22] S. Saisorn, S. Wongwises, The effects of channel diameter on flow pattern, void fraction and pressure drop of two-phase air-water flow in circular micro-channels, Exp. Therm. Fluid Sci. 34 (2010) 454-462.
[23] G.L. Morini, Single-phase convective heat transfer in microchannels: a review of experimental results, Int. J. Therm. Sci. 43 (2004) 631-651.
[24] M. Sahimi, Flow and transport in porous media and fractured rock: from classical methods to modern approaches, second ed., John Wiley & Sons2011.
[25] E.W. Washburn, The dynamics of capillary flow., Phys. Rev. 17 (1921) 273-283.
[26] F.A.L. Dullien, Porous Media Fluid transport and pore structure, second ed., Academic Press, San Diego, 1992.
[27] P.M.Y. Chung, M. Kawaji, The effect of channel diameter on adiabatic two-phase flow characteristics in microchannels, Int. J. Multiph. Flow 30 (2004) 735-761.
[28] J. Yue, G.W. Chen, Q. Yuan, Pressure drops of single and two-phase flows through T-type microchannel mixers, Chem. Eng. J. 102 (2004) 11-24.
[29] L.C. Sun, K. Mishima, Evaluation analysis of prediction methods for two-phase flow pressure drop in mini-channels, Int. J. Multiph. Flow 35 (2009) 47-54.
[30] R.S. Stanley, R.F. Barron, T.A. Ameel, Two-phase flow in microchannels, J. Microelectromech. Syst. DSC-Vol. 62/HTD-Vol. 354 (1997) 143-152.
[31] A. Kawahara, P.M.Y. Chung, M. Kawaji, Investigation of two-phase flow pattern, void fraction and pressure drop in a microchannel, Int. J. Multiph. Flow

28 (2002) 1411-1435.
[32] H. Ju Lee, S. Yong Lee, Pressure drop correlations for two-phase flow within horizontal rectangular channels with small heights, Int. J. Multiph. Flow 27 (2001) 783-796.
[33] N.J. English, S.G. Kandlikar, An experimental investigation into the effect of surfactants on air-water two-phase flow in minichannels, Heat Transf. Eng. 27 (2006) 99-109.
[34] D.L. Albernaz, F.R. Cunha, Unsteady motion of a spherical bubble in a complex fluid: Mathematical modelling and simulation, Appl. Math. Model. 37 (2013) 8972-8984.
[35] T. Cubaud, C.M. Ho, Transport of bubbles in square microchannels, Phys. Fluids 16 (2004) 4575-4585.
[36] F.Q. Song, Y.S. Xu, H.M. Li, Blood flow in capillaries by using porous media model, J. Cent. South Univ. Technol. 14 (2007) 46-49.
[37] X.X. Li, X.F. Fan, S. Brandani, Difference in pore contact angle and the contact angle measured on a flat surface and in an open space, Chem. Eng. Sci. 117 (2014) 137-145.
[38] M.T. Kreutzer, F. Kapteijn, J.A. Moulijn, C.R. Kleijn, J.J. Heiszwolf, Inertial and interfacial effects on pressure drop of Taylor flow in capillaries, AICHE J. 51 (2005) 2428-2440.
[39] O. Vizika, D.G. Avraam, A.C. Payatakes, On the Role of the Viscosity Ratio during Low-Capillary-Number Forced Imbibition in Porous-Media, J. Colloid Interface Sci. 165 (1994) 386-401.
[40] D.R. Chakrabarti, G. Das, S. Ray, Pressure drop in liquid-liquid two phase horizontal flow: Experiment and prediction, Chem. Eng. Technol. 28 (2005) 1003-1009.
[41] F. Fairbrother, A.E. Stubbs, 119. Studies in electro-endosmosis. Part VI. The “bubble-tube” method of measurement, J. Chem. Soc. 0 (1935) 527-529.
[42] F.P. Bretherton, The Motion of Long Bubbles in Tubes, J. Fluid Mech. 10 (1961) 166-188.
[43] M.J.F. Warnier, M.H.J.M. de Croon, E.V. Rebrov, J.C. Schouten, Pressure drop of gas–liquid Taylor flow in round micro-capillaries for low to intermediate Reynolds numbers, Microfluid. Nanofluid. 8 (2009) 33-45.
[44] T. Harirchian, Two-phase flow and heat transfer in microchannels, Purdue University 2010.
[45] R.W. Lockhart, R.C. Martinelli, Proposed correlation of data for isothermal two-phase, two-component flow in pipes, Chem. Eng. Prog 45 (1949) 39-48.
[46] X.X. Li, X.F. Fan, A. Askounis, K.J. Wu, K. Sefiane, V. Koutsos, An experimental study on dynamic pore wettability, Chem. Eng. Sci. 104 (2013) 988-997.
[47] G.F. Hewitt, G.L. Shires, T.R. Bott, Process heat transfer, CRC [etc], Boca Raton, Fla., 1993.
[48] L. Friedel, Two-phase Flow in Pipelines and Heat Exchangers, Chem. Ing. Tech. 56 (1984) 17-17.

[49] M. Stange, M.E. Dreyer, H.J. Rath, Capillary driven flow in circular cylindrical tubes, Phys. Fluids 15 (2003) 2587-2601.
[50] N. Ichikawa, K. Hosokawa, R. Maeda, Interface motion of capillary-driven flow in rectangular microchannel, J. Colloid Interface Sci. 280 (2004) 155-164.
[51] B.H. Cheong, T.W. Ng, Y. Yu, O.W. Liew, Using the meniscus in a capillary for small volume contact angle measurement in biochemical applications, Langmuir 27 (2011) 11925-11929.
[52] A. Cioncolini, J.R. Thome, C. Lombardi, Unified macro-to-microscale method to predict two-phase frictional pressure drops of annular flows, Int. J. Multiph. Flow 35 (2009) 1138-1148.
[53] W.H. McAdams, Heat transmission, third ed., McGraw-Hill, New York, 1954.
[54] C.L. A. Cicchitti, M. Silvestri, G. Solddaini, R. Zavalluilli, Two-phase cooling experiments–Pressure drop, heat transfer and burnout measurement, Energia Nucl. 7 (1960) 407-425.
[55] A.E. Dukler, M. Wicks, R.G. Cleveland, Frictional pressure drop in two-phase flow: A. A comparison of existing correlations for pressure loss and holdup, AICHE J. 10 (1964) 38-43.
[56] D.R.H. Beattie, P.B. Whalley, A simple two-phase frictional pressure drop calculation method, Int. J. Multiph. Flow 8 (1982) 83-87.
[57] S. Lin, C.C.K. Kwok, R.Y. Li, Z.H. Chen, Z.Y. Chen, Local Frictional Pressure-Drop during Vaporization of R-12 through Capillary Tubes, Int. J. Multiph. Flow 17 (1991) 95-102.
[58] K. Mishima, T. Hibiki, Some characteristics of air-water two-phase flow in small diameter vertical tubes, Int. J. Multiph. Flow 22 (1996) 703-712.
[59] P.G. M. Suo, Two-phase flow in capillary tubes, J. Basic Eng. 86 (1964) 576-582.
[60] T. Metz, W. Streule, R. Zengerle, P. Koltay, StarTube: a tube with reduced contact line for minimized gas bubble resistance, Langmuir 24 (2008) 9204-9206.